

## Article

# Insights into the Reactivation Process of Thermal Aged Bimetallic Pt-Pd/CeO<sub>2</sub>-ZrO<sub>2</sub>-La<sub>2</sub>O<sub>3</sub> Catalysts at Different Treating Temperatures and Their Structure–Activity Evolutions for Three-Way Catalytic Performance

Jie Wan <sup>1,2,\*</sup>, Kai Chen <sup>2</sup>, Qi Sun <sup>1,3</sup>, Yuanyuan Zhou <sup>1,4</sup>, Yanjun Liu <sup>1</sup>, Jin Zhang <sup>1</sup>, Jiancong Dong <sup>1</sup>, Xiaoli Wang <sup>3</sup>, Gongde Wu <sup>1</sup> and Renxian Zhou <sup>2,\*</sup>

<sup>1</sup> Energy Research Institute, Nanjing Institute of Technology, Nanjing 211167, China; sunnqi@163.com (Q.S.); zhoyuanyuanxxh@163.com (Y.Z.); yjliu@njit.edu.cn (Y.L.); zhangjinnuaa@njit.edu.cn (J.Z.); jcdong@njit.edu.cn (J.D.); wugongde@njit.edu.cn (G.W.)

<sup>2</sup> Institute of Catalysis, Zhejiang University, Hangzhou 310028, China; kaichen@nyu.edu

<sup>3</sup> School of Environmental Engineering, Nanjing Institute of Technology, Nanjing 211167, China; wangxiaoli212@njit.edu.cn

<sup>4</sup> School of Materials Science and Engineering, Ocean University of China, Qingdao 266100, China

\* Correspondence: jwan@njit.edu.cn (J.W.); zhorenxian@zjut.edu.cn (R.Z.)

**Abstract:** CeO<sub>2</sub>-ZrO<sub>2</sub>-La<sub>2</sub>O<sub>3</sub> supported Pt-Pd bimetallic three-way catalysts (0.6Pt-0.4Pd/CZL) were synthesized through the conventional impregnation method and then subjected to severe thermal aging. Reactivating treatments under different temperatures were then applied to the aged catalysts above. Three-way catalytic performance evaluations and dynamic operation window tests along with detailed physio-chemical characterizations were carried out to explore possible structure–activity evolutions during the reactivating process. Results show that the reactivating process conducted at proper temperatures (500–550 °C) could effectively restore the TWC catalytic performance and widen the operation window width. The suitable reactivating temperature ranges are mainly determined by the decomposing temperature of PMO<sub>x</sub> species, the thermal stability of PM-O-Ce species, and the encapsulation temperature of precious metals by CZL support. Reactivating under appropriate temperature helps to restore the interaction between Pt and CZL support to a certain extent and to re-expose part of the encapsulated precious metals. Therefore, the dynamic oxygen storage/release capacity, redox ability, as well as thermal stability of PtO<sub>x</sub> species, can be improved, thus benefiting the TWC catalytic performances. However, the excessively high reactivating temperature would cause further embedment of Pd by CZL support, thus leading to a further decrease in both dynamic oxygen storage/release capacity and the TWC catalytic performance after reactivating treatment.

**Keywords:** three-way catalyst; Pt/Pd bimetallic catalyst; metal–support interaction; thermal ageing; reactivating process



**Citation:** Wan, J.; Chen, K.; Sun, Q.; Zhou, Y.; Liu, Y.; Zhang, J.; Dong, J.; Wang, X.; Wu, G.; Zhou, R. Insights into the Reactivation Process of Thermal Aged Bimetallic Pt-Pd/CeO<sub>2</sub>-ZrO<sub>2</sub>-La<sub>2</sub>O<sub>3</sub> Catalysts at Different Treating Temperatures and Their Structure–Activity Evolutions for Three-Way Catalytic Performance. *Catalysts* **2024**, *14*, 299. <https://doi.org/10.3390/catal14050299>

Academic Editor: Carlo Santoro

Received: 8 April 2024

Revised: 27 April 2024

Accepted: 30 April 2024

Published: 1 May 2024



**Copyright:** © 2024 by the authors. Licensee MDPI, Basel, Switzerland. This article is an open access article distributed under the terms and conditions of the Creative Commons Attribution (CC BY) license (<https://creativecommons.org/licenses/by/4.0/>).

## 1. Introduction

The fast-developing modern car industry has brought great convenience to people's daily lives but the air pollution caused by automobile exhaust has posed a great threat to both human health and environmental sustainability [1,2]. Three-way catalysts can simultaneously eliminate three major pollutants from automobile exhaust including carbon monoxide (CO), hydrocarbons (HCs), and nitrogen oxides (NO<sub>x</sub>) and have been widely employed as the most effective after-treatment technique for automobile pollution control [3,4]. Typical TWC catalysts generally consist of precious metals (PM, such as Pt, Pd, and Rh),  $\gamma$ -Al<sub>2</sub>O<sub>3</sub>, and CeO<sub>2</sub>-ZrO<sub>2</sub> supporting materials [5], among which Pt and Pd are the most essential active components.

As one of the earliest generations applied for three-way catalysis (TWC), Pt-based catalysts have an outstanding oxidation ability. However, they are known to have worse conversion performance than NO and are prone to sintering clearly [6]. On the other hand, Pd-based catalysts exhibit exceptional CO oxidation ability as same as and better than the thermostability with respect to Pt. This has led to extensive research on Pd-based catalysts in recent decades [7]. However, the Pd price has been steadily increasing and has surpassed the Pt in the past few years. As a result, there is a growing demand for the amount of Pd used in TWC catalysts. Therefore, the development of novel Pt-Pd bimetallic catalysts could potentially reduce raw material costs while at the same time, the TWCs could still maintain superior catalytic performance. Several studies [8,9] have demonstrated that constructing bimetallic catalysts can create a synergistic effect between two active components, leading to the modulation of physio-chemical properties and thereby enhancing the activity and stability of catalysts. For instance, Lim et al. [10] reported that bimetallic nano dendrites such as Pt-Pd exhibited outstanding catalytic performance for oxygen reduction reactions because of their large specific surface area and highly active crystal plane exposure. Additionally, Jin et al. [11] found that TiO<sub>2</sub>-supported alloy-type Pt-Pd bimetallic catalysts demonstrated superior catalytic activity and selectivity for oxidizing glucose as the comparison of Pt-only catalysts. In our previous studies [12], bimetallic Pt-Pd/CeO<sub>2</sub>-ZrO<sub>2</sub>-La<sub>2</sub>O<sub>3</sub> catalysts with optimized Pt/Pd ratios also exhibited outstanding three-way catalytic performance and expanded operation temperature window width.

The increasingly stringent exhaust regulations in recent years have pushed forward the demand for developing close-coupled TWCs, where the TWC converter is installed close to the engine's exhaust ports or even within the exhaust manifold. Such close-coupled TWCs often experience high temperatures up to 900~1000 °C, which raises new challenges to the extremely high thermal stability of the TWC catalysts. Deactivations of TWC catalysts due to such thermal aging after long-term operation are inevitable, which are manifested by the increase in the particle size of the support, the agglomeration of PM particles, and the decrease in the oxygen storage/releasing capacity and loss of catalytic activity [13]. Many recent research works proposed that treating the aged catalysts under an oxidizing (O<sub>2</sub> dominating) atmosphere (also known as "reactivation") can be one promising way to recover the deteriorated TWC activity [14,15]. Hickey et al. [16] reported that the catalytic activity of Pd/Ce<sub>0.68</sub>Zr<sub>0.32</sub>O<sub>2</sub> catalysts treated at high temperatures in an oxidizing atmosphere was greatly restored and further characterizations showed that the chemical states and nanostructures of both the precious metals and Ce<sub>0.68</sub>Zr<sub>0.32</sub>O<sub>2</sub> support were significantly changed. Nagai et al. [17] demonstrated that the Pt dispersion and TWC activity of aged Pt/CeO<sub>2</sub>-ZrO<sub>2</sub>-Y<sub>2</sub>O<sub>3</sub> can be significantly improved by treating in a 20% O<sub>2</sub>-He atmosphere and the following in situ XAS and in situ TEM observation indicated that the interaction between Pt and Ce can induce atomic migration, which led to the redispersion of Pt dispersion. However, the effect of such a reactivation process on the bimetallic TWC systems remains unclear and is relatively less studied.

In the current work, Pt-Pd bimetallic catalysts supported by CeO<sub>2</sub>-ZrO<sub>2</sub>-La<sub>2</sub>O<sub>3</sub> mixed oxides (Pt-Pd/CZL) were synthesized and underwent severe thermal aging. Reactivating treatments under different temperatures were then applied to these aged catalysts above. The obtained catalysts underwent evaluations for the performance of three-way catalytic properties and were further characterized through various techniques including HRTEM, XPS, H<sub>2</sub>-TPR, and DOSC as well as O<sub>2</sub>-TPSR methods. This paper is focused on exploring the optimum reactivation temperature under simulated conditions close to actual working conditions. Additionally, it aims to investigate the physicochemical properties and catalytic behaviors through the reactivating process effects to gain new insights into how the structure-activity correlation of Pt-Pd/CZL bimetallic catalysts evolves during the aging and reactivating process.

## 2. Results and Discussion

### 2.1. Three-Way Catalytic Activity Evaluation

Figure 1 presents the TWC light-off curves of all the obtained Pt-Pd bimetallic catalysts (fresh, thermal-aged, and reactivated at different temperatures) under the ideal air-to-fuel ratio ( $\lambda = 1$ ). The corresponding  $T_{10\%}/T_{50\%}/T_{90\%}$  (the temperature when conversion of pollutant reaches 10%/50%/90%) histograms are shown in Figure 2. It can be seen that the catalytic activity of reactivated catalysts varies quite a lot with different reactivating temperatures. As reactivation temperature ranged from 500 °C to 600 °C, the  $T_{50\%}$  for HCs oxidation stayed almost the same while  $T_{90\%}$  decreased slightly; while the catalytic activity for CO oxidation and NO reduction can be dramatically recovered, the  $T_{50\%}$  and  $T_{90\%}$  for NO conversion both especially dropped by about 50 °C compared to the aged catalysts. However, continuing to increase the reactivation temperature brought no benefits but rather more severe deteriorated activity. As for either the 0.6Pt-0.4Pd/CZL-a (R650) or 0.6Pt-0.4Pd/CZL-a (R700) sample, a drastic increase in  $T_{50\%}/T_{90\%}$  values for NO conversion can be observed while slight deterioration can be seen for HC and CO oxidation. Hence, on the one hand, it can be proposed that the optimum reactivation temperature for 0.6Pt-0.4Pd/CZL-a should be below 600 °C. On the other hand, the NO reduction activity is most sensitive to the reactivation temperature. It is observed from Figure 1 that the 550 °C reactivation could only slightly improve HC conversion for the aged 0.6Pt-0.4Pd/CZL sample. This can be hard to interpret because the HC oxidation reaction has many complex factors affected. Here, we propose a possible explanation that the low carbon alkane/alkene oxidation over PM/CeO<sub>2</sub> catalysts follows the Mars-van Krevelen mechanism, which proves the lattice oxygen migration and participation are crucial. CZL support was severely sintered/agglomerated during 1000 °C thermal aging, while, conversely, the reactivation process had no significant effect on (or in other words, was not able to recover) the CZL support's textural structure (as 'Section 2.3. HRTEM and EDS Analysis' supported), leading to a deterioration in the participation of lattice oxygen even after reactivation. Therefore, the reactivated 0.6Pt-0.4Pd/CZL-a(R550) sample shows only a very slight recovery in HC conversion. Additionally, Table S1 shows that effective reactivation of deactivated TWCs generally requires a chlorine-containing atmosphere, which can cause secondary pollution because they are toxic and prone. This result, as a harmless oxygen gas mixture applied, can provide positive support for developing green and effective regeneration methods for TWCs.

Moreover, more details regarding the reaction process can be found based on the light-off curves. By comparing fresh 0.6Pt-0.4Pd/CZL and catalysts reactivated within 500 °C to 600 °C, we can see similar shapes of the light-off curves for all three pollutants, which suggests that the fundamental reaction process for HC, CO, and NO might be the same for these catalysts and only the temperatures at which the conversion begins are different. However, for aged 0.6Pt-0.4Pd/CZL-a, 0.6Pt-0.4Pd/CZL-a (R650), and 0.6Pt-0.4Pd/CZL-a (R700), these three samples present a similar flatten plateau for both HC and NO conversion at around 260 °C. With increasing reaction temperatures, NO conversion on 0.6Pt-0.4Pd/CZL-a increased immediately, while NO conversion on 0.6Pt-0.4Pd/CZL-a (R650) and 0.6Pt-0.4Pd/CZL-a (R700) still rose quite slowly until the reaction temperature exceeds 300 °C. These interesting phenomena might give us hints that HC and NO would undergo a simultaneous conversion on 0.6Pt-0.4Pd/CZL-a, 0.6Pt-0.4Pd/CZL-a (R650), and 0.6Pt-0.4Pd/CZL-a (R700) below 260 °C, while such a synchronized reaction process changes at higher temperature regarding different catalysts.

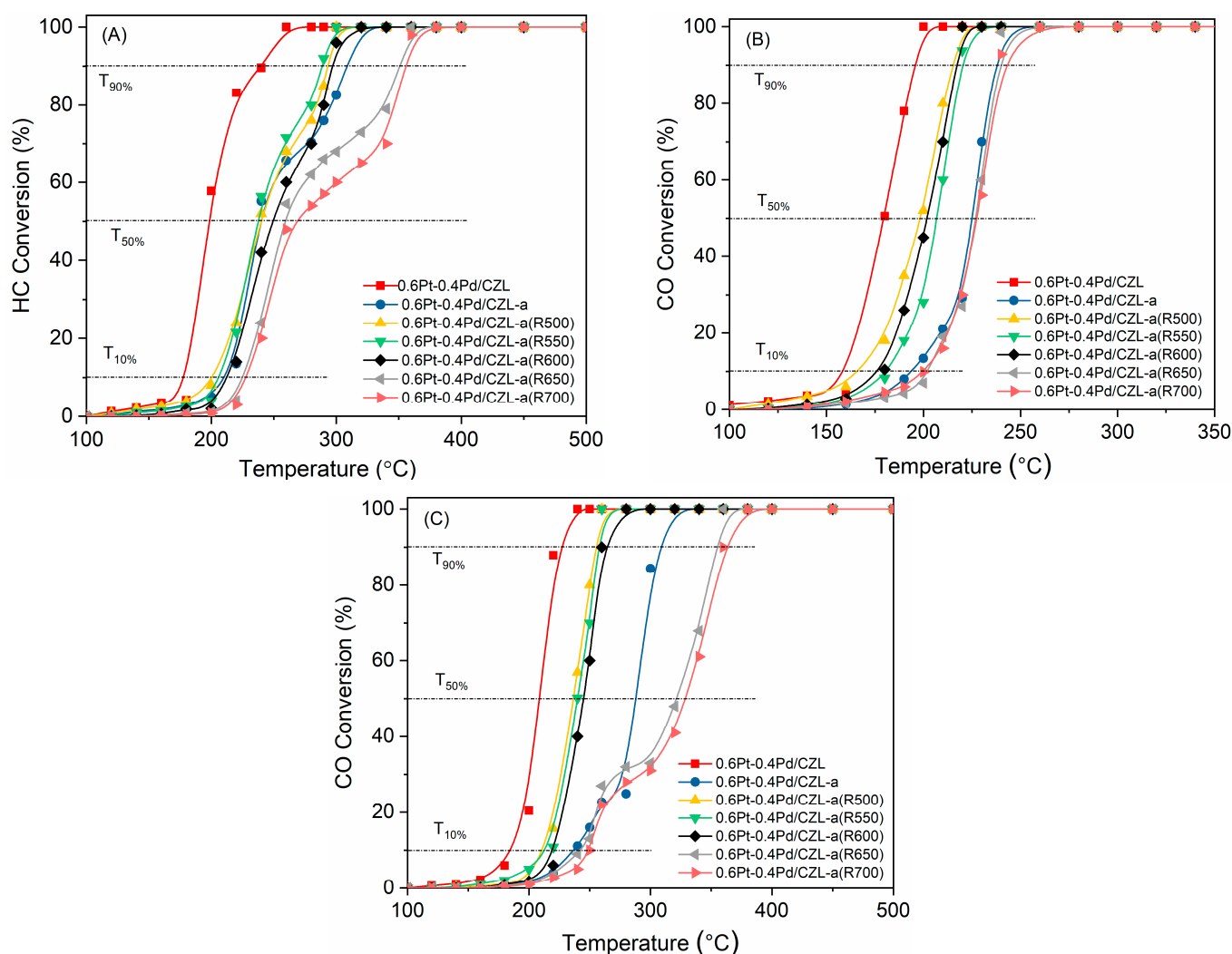


**Figure 1.** The light-off curves of the fresh, aged, and reactivated 0.6Pt-0.4Pd/CZL catalysts toward HC (A), CO (B), and NO (C).

## 2.2. Dynamic Operation Window Tests

The operational dynamics of the 0.6Pt-0.4Pd/CZL catalysts, whether in a fresh, aged, or reactivated condition, were evaluated by the concentrations of CO + N<sub>2</sub> and NO monitored over time under fluctuating air/fuel ratios when  $\lambda = 0.90$  and 1.15. As Figure 3 depicts, a rapid decrease in CO concentration occurs within approximately 2 min after the  $\lambda = 0.90$  shift to 1.15 for entire samples, resulting in a new plateau established. This behavior can be attributed to the low activation energy and fast reaction rate belonging to the “CO + O<sub>2</sub>” oxidation reaction [18,19]. Subsequently, within a 3 to 10-min timeframe range, another plateau emerges when the N<sub>2</sub> concentration declines, which is related to the hindered NO conversion (see the increasing NO concentration in Figure 3B) caused by the dominating CO oxidation reaction. When  $\lambda$  is switched back to 0.90, the CO concentration increases to form a plateau after around 10 min due to the depletion of stored bulk oxygen. We propose that the  $\lambda$  switching at time duration within 0.90 to 1.15 ranges, associated with the NO concentration plateau, denotes the catalyst’s dynamic operation window width, namely the later the NO plateau appears, the wider the catalyst’s dynamic operation window. According to Figure 3, the widest dynamic operation window appeared on the fresh 0.6Pt-0.4Pd/CZL exhibits while it was drastically narrowed after thermal aging. Meanwhile, the dynamic operation window width of the reactivated catalysts varies with different reactivation temperatures. For these reactivated below 600 °C, the dynamic operation win-

dow can be widened compared to 0.6Pt-0.4Pd/CZL-a, especially for the 0.6Pt-0.4Pd/CZL-a (R550) sample. However, as the reactivation temperature increased, the dynamic operation window width of the reactivated catalyst gradually narrowed and eventually became approximately the same as that of the aged catalyst. Since the dynamic operation window of the catalyst is fundamentally determined by its oxygen storage/release capacity, these results indicate that the reactivation at an appropriate temperature can partially restore the oxygen storage and release capacity of the catalyst but such recovery is limited to a certain extent.

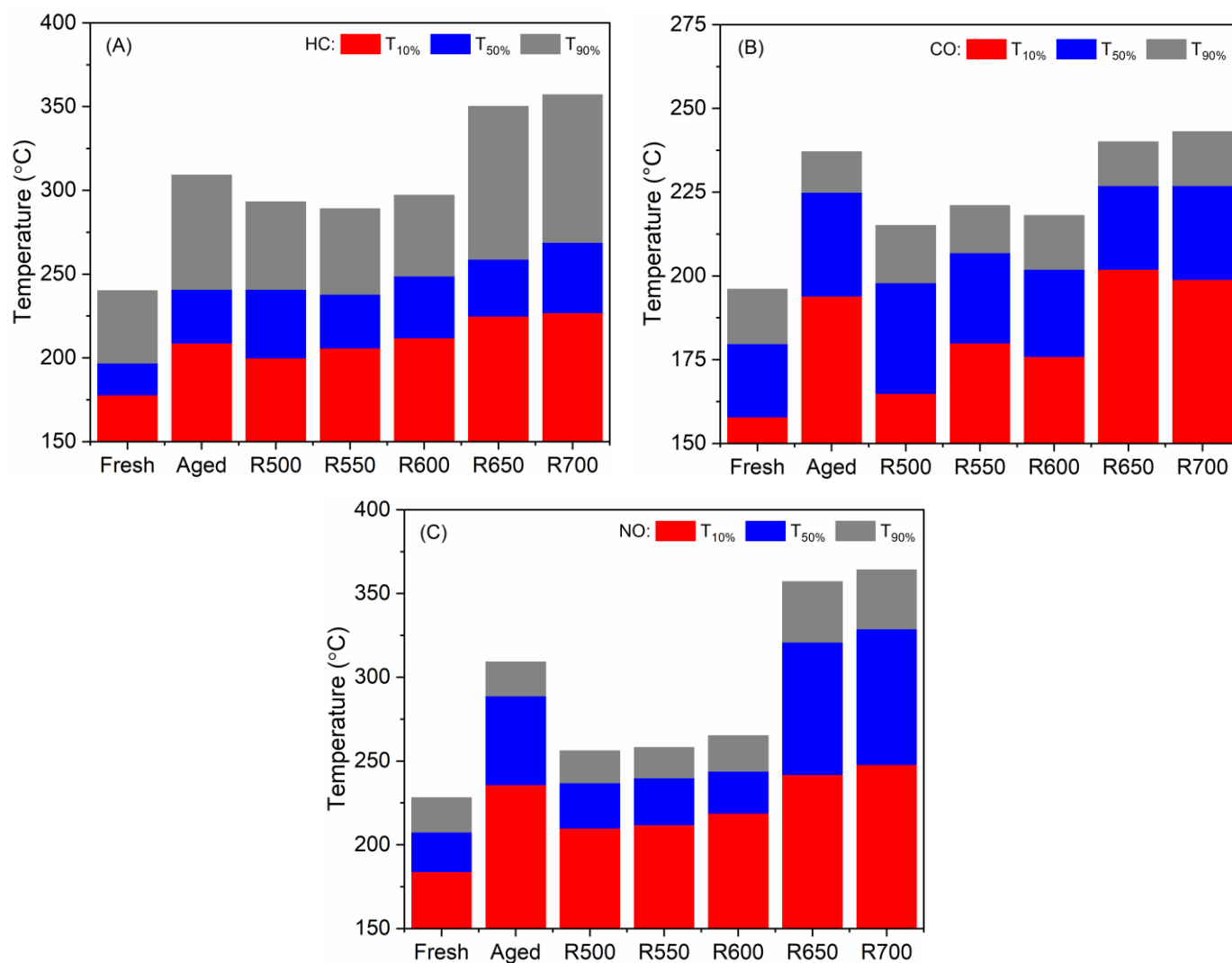


**Figure 2.** The values of T<sub>10%</sub>, T<sub>50%</sub>, and T<sub>90%</sub> of the fresh, aged, and reactivated 0.6Pt-0.4Pd/CZL catalysts towards HC (A), CO (B), and NO (C).

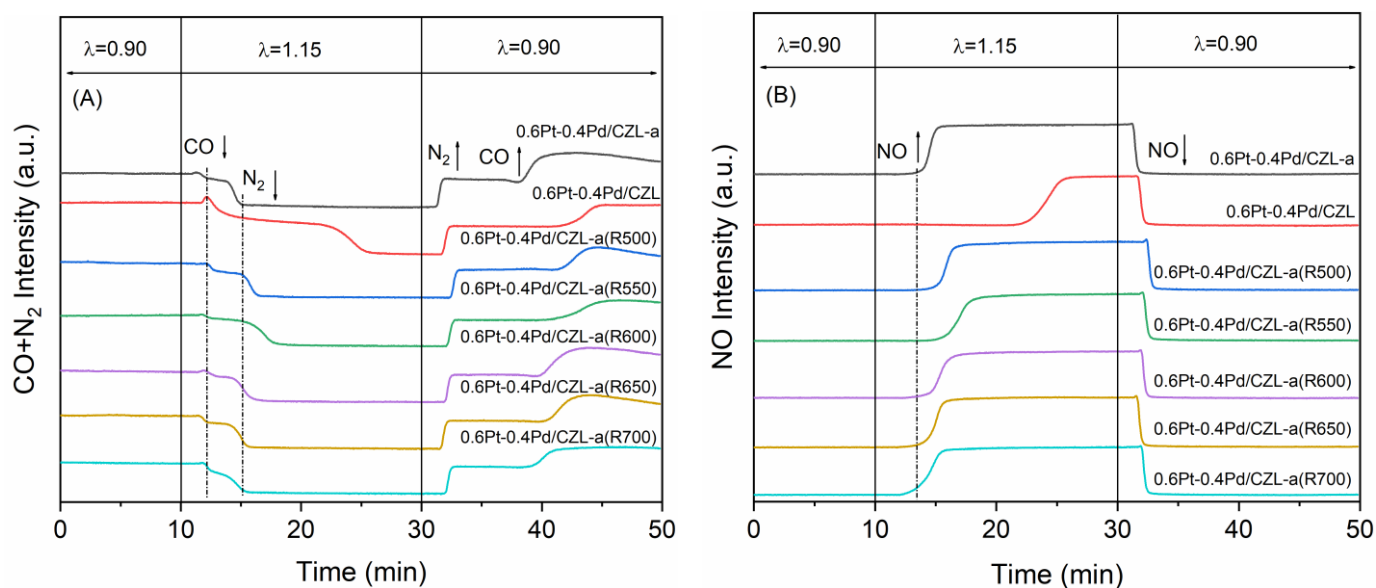


**Figure 3.** Concentration curves of CO + N<sub>2</sub> (A) and NO (B) over the fresh, aged, and reactivated 0.6Pt-0.4Pd/CZL catalysts as a function of time under air/fuel ratio fluctuating conditions.

### 2.3. HRTEM and EDS Analysis

The 0.6Pt-0.4Pd/CZL, 0.6Pt-0.4Pd/CZL-a, 0.6Pt-0.4Pd/CZL-a(R550), and 0.6Pt-0.4Pd/CZL-a(R700) were observed by HRTEM and the record images were displayed in Figure 4. The CZL supports of the fresh 0.6Pt-0.4Pd/CZL catalyst exhibited polygonal shapes with a 10 nm particle size, as determined by the interplanar spacing value analysis indicating that the (111), (110), and (100) planes are exposed crystal planes [20]. After 1000 °C thermal aging for 2 h, the 0.6Pt-0.4Pd/CZL-a particle size significantly increased from approximately 10 nm to 16 nm, distracting from the fact that relatively severe sintering and agglomeration occurred during this process, which could be one of the main reasons for the decreasing oxygen storage and release capacity. For the reactivated 0.6Pt-0.4Pd/CZL-a(R550) and 0.6Pt-0.4Pd/CZL-a(R700) samples, no obvious changes could be seen regarding either the particle sizes or the exposed crystal planes of CZL supports. XRD analysis (see Figure S2 in the Supplementary Material) also revealed that the reactivated 0.6Pt-0.4Pd/CZL-a(R550) presented a characteristic cubic CeO<sub>2</sub>-ZrO<sub>2</sub> phase (JCPDS# 38-1439) compared to the fresh 0.6Pt-0.4Pd/CZL and aged 0.6Pt-0.4Pd/CZL-a samples. These results indicated the meaning that the reactivation process had no significant effect on the textural structure of the CZL supports. Furthermore, the verification of Pt and Pd particles in the bimetallic catalysts through HRTEM observation could be challenging because of their low loading amount. Therefore, EDS mapping scans were conducted for a better understanding of the PM particles' surface distributions. As Figure 4 shows, when the thermal aging finished, these precious metals continued to disperse uniformly on the catalyst surface rather than the large agglomerates formed. This may be connected with the formation of well-reported PM-O-Ce species due to the strong metal-support interaction, which could anchor the PM particles on the CZL surface and effectively inhibit the sintering of precious metal during thermal aging. For the reactivated 0.6Pt-0.4Pd/CZL-a(R550) and 0.6Pt-0.4Pd/CZL-a(R700) samples, no trace of significant changes for PM dispersion states were found after reactivation. These results suggest that the different activity recovery after reactivation might not originate from either the structure of CZL supports or the PM dispersion states.

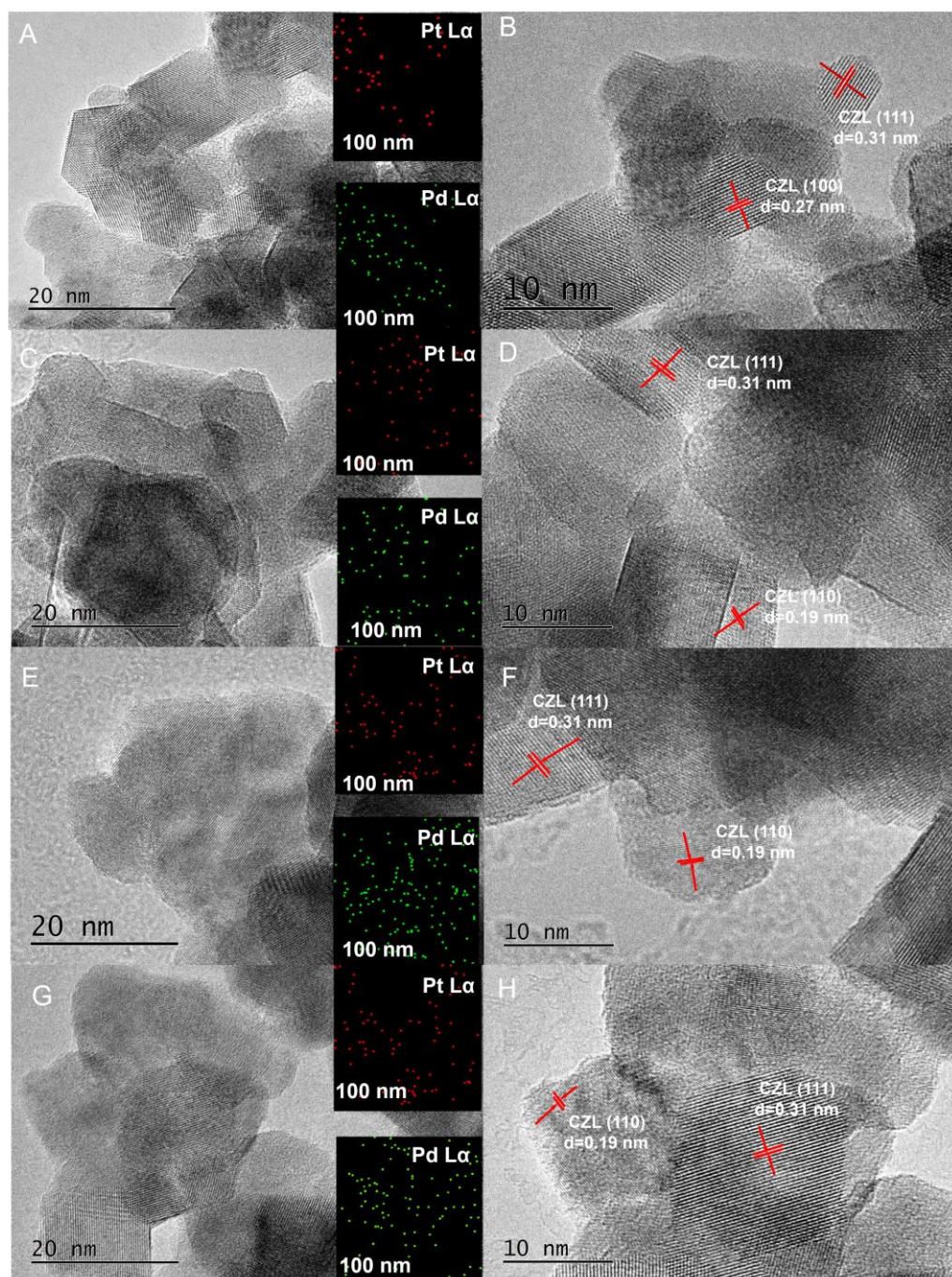


**Figure 4.** HRTEM images and STEM-EDS mapping images of (A,B) 0.6Pt-0.4Pd/CZL, (C,D) 0.6Pt-0.4Pd/CZL-a, (E,F) 0.6Pt-0.4Pd/CZL-a(R550), and (G,H) 0.6Pt-0.4Pd/CZL-a(R700).

#### 2.4. Chemical States of Surface Elements by XPS

The chemical states of surface elements including Pt, Pd, and Ce were investigated by XPS (Figure 5) and the quantitative results based on peak decomposition are listed in Table 1. The Pt 4f spectra shown in Figure 5A could be decomposed into six parts: peaks centered at 70.9 eV and 74.2 eV represent characteristics peaks of the Pt<sup>0</sup> species and peaks at 72.6 eV and 75.9 eV are assigned to the Pt<sup>2+</sup> species, while those located at 74.4 eV and 77.8 eV are attributed to the Pt<sup>4+</sup> species. For the fresh 0.6Pt-0.4Pd/CZL catalyst, only a very small portion of Pt<sup>0</sup> species can be observed. After thermal aging at 1000 °C, the surface Pt<sup>0</sup> content increased significantly and the (Pt<sup>2+</sup> + Pt<sup>4+</sup>)/Pt ratio dropped from 92.1% to about 52.6%. This indicates that the Pt-O-Ce species formed between Pt and

CZL support were partially destructed during high-temperature thermal aging. For the reactivated samples, the surface  $\text{Pt}^0$  content of 0.6Pt-0.4Pd/CZL-a(R550) slightly decreased while  $\text{Pt}^{4+}$  content was largely increased, suggesting the re-oxidation of surface Pt during reactivation in oxygen atmospheres. However, continuing to ramp reactivating temperature, the surface  $\text{Pt}^0$  content of the 0.6Pt-0.4Pd/CZL-a(R700) increased again compared with 0.6Pt-0.4Pd/CZL-a. Figure 5B presents the Pd 3d spectra and four major peaks can be observed, as the peaks at 335.0 eV, 341.1 eV, 337.3 eV, and 343.0 eV are assigned to  $\text{Pd}^0$  3d<sub>3/2</sub>,  $\text{Pd}^0$  3d<sub>5/2</sub>,  $\text{Pd}^{2+}$  3d<sub>3/2</sub>, and  $\text{Pd}^{2+}$  3d<sub>5/2</sub>, respectively [21]. Being different from the Pt content, the fresh 0.6Pt-0.4Pd/CZL showed relatively higher initial  $\text{Pd}^0$  content and it increased quite slightly after thermal aging, which could be related to the relatively high decomposition temperature of PdO. Nevertheless, similar trends in  $\text{Pd}^0$ - $\text{Pd}^{2+}$  evolution can be observed between the aged and reactivated samples, as surface  $\text{Pd}^0$  content of 0.6Pt-0.4Pd/CZL-a clearly dropped after reactivation at 550 °C and slightly increased again after 700 °C reactivation. Overall, these results demonstrate that the strong metal–support interaction was partially sabotaged to form metallic PM species during thermal aging. Reactivation at appropriate temperatures can re-establish such an interaction and turn the metallic PM back to the oxidized state but it could contrarily promote more formation of metallic PM species when the reactivation temperature is too high.

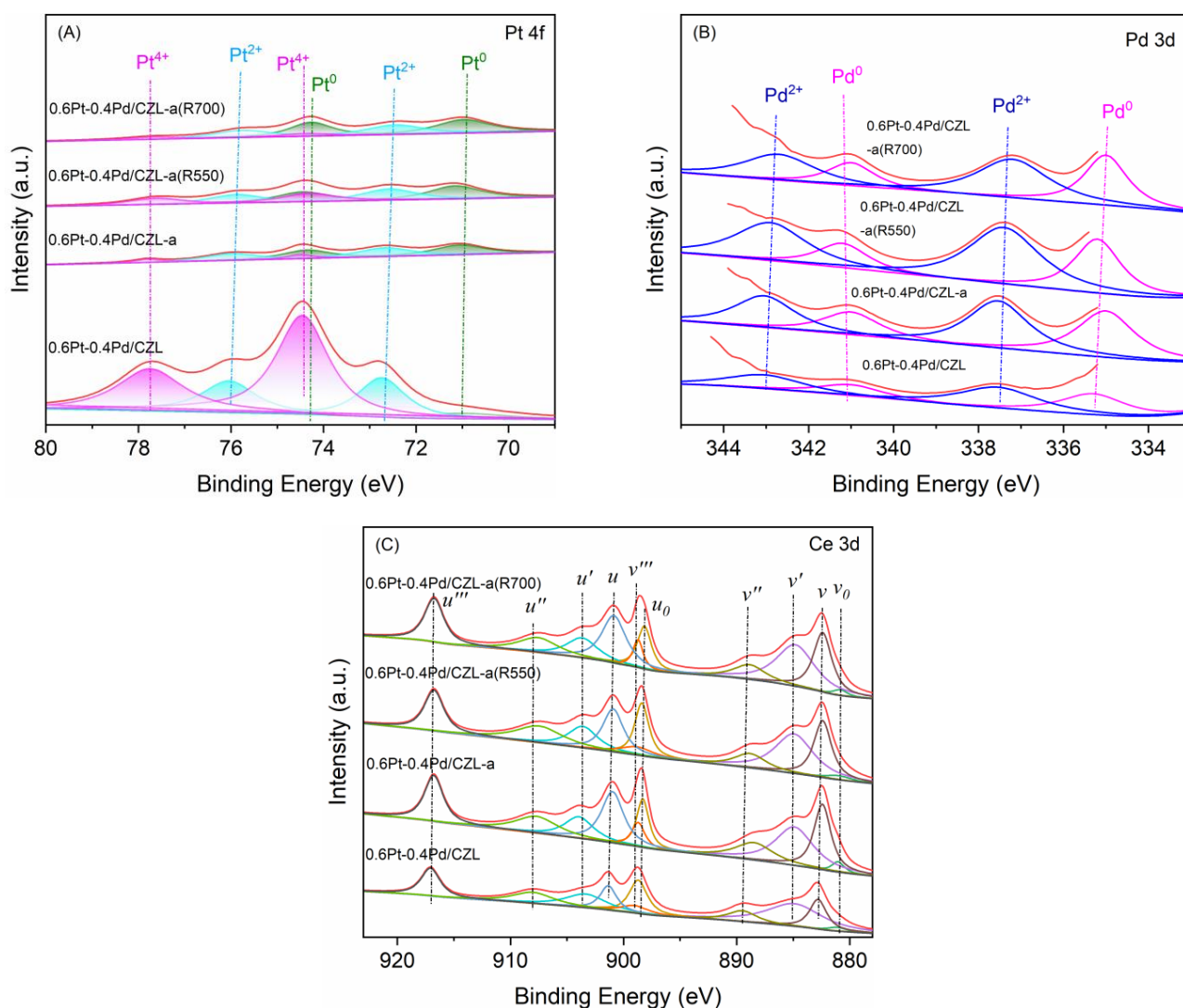


**Figure 5.** XPS spectra of (A) Pt 4f, (B) Pd 3d, and (C) Ce 3d of the 0.6Pt-0.4Pd/CZL, 0.6Pt-0.4Pd/CZL-a, 0.6Pt-0.4Pd/CZL-a(R550), and 0.6Pt-0.4Pd/CZL-a(R700) catalysts.

**Table 1.** Surface element contents of the fresh, aged, and reactivated 0.6Pt-0.4Pd/CZL catalysts derived from XPS analyses.

Samples	Surface Composition (at. %)		Pt <sup>0</sup> /Pt (%)	Pt <sup>2+</sup> /Pt (%)	Pt <sup>4+</sup> /Pt (%)	Pd <sup>0</sup> /Pd (%)	Pd <sup>2+</sup> /Pd (%)	Ce <sup>3+</sup> /Ce (%)
	Pt	Pd						
0.6Pt-0.4Pd/CZL	0.14	0.13	7.9	28.2	63.9	43.0	57.0	45.2
0.6Pt-0.4Pd/CZL-a	0.04	0.39	47.4	43.2	9.4	45.3	54.7	38.7
0.6Pt-0.4Pd/CZL-a(R550)	0.07	0.50	39.5	39.9	20.6	35.7	64.3	42.5
0.6Pt-0.4Pd/CZL-a(R700)	0.04	0.25	52.0	37.9	10.1	41.1	58.9	36.9

The Ce 3d spectra are displayed in Figure 5C. In the case of the fresh 0.6Pt-0.4Pd/CZL catalyst, 10 characteristic peaks were observable and could be divided into two series named *u* series and *v* series, which stem from different Ce oxidation states with the 3d<sub>3/2</sub> and 3d<sub>5/2</sub> split-orbit multiplex lines, respectively. Among these characteristic peaks [22], Ce<sup>3+</sup> related lines were identified as *u*<sub>0</sub> (899.1 ± 0.2 eV), *u*' (903.4 ± 0.2 eV), *v*<sub>0</sub> (880.9 ± 0.2 eV), and *v*' (885.2 ± 0.2 eV). The Ce<sup>3+</sup> content decreased after thermal aging and increased again upon reactivation at 550 °C but it could not go back to the original level of fresh catalyst. Reactivation at high temperatures caused a continuous drop of Ce<sup>3+</sup> content of 0.6Pt-0.4Pd/CZL-a(R700). Various studies have pointed out that the surface Ce<sup>3+</sup> content could be positively correlated with the concentration of oxygen vacancies [23], which helped further affect the dynamic oxygen storage and release capacity, thus explaining the similar evolving trend of the dynamic operation window above.

Moreover, we could see from Table 1 that the surface Pt content was obviously lowered after thermal aging, which was due to the encapsulation of Pt by the CZL carrier during the aging process. Reactivating under an oxidizing atmosphere at an appropriate temperature could partially re-expose the encapsulated Pt particles to the catalyst's surface [24]; therefore, surface Pt content of the 0.6Pt-0.4Pd/CZL-a(R550) increased after reactivation. On the contrary, the surface Pd content increased after aging. The encapsulation of Pd generally occurred under a redox atmosphere at higher temperatures compared to that of Pt according to previous studies by Wang et al. [25]; thus, the increased surface Pd content of 0.6Pt-0.4Pd/CZL-a might be related to the break of Pt-Pd heterostructure (reported in our previous study) in the fresh sample and the exudation of Pd to CZL surface. After reactivating at 550 °C, the surface Pd content of 0.6Pt-0.4Pd/CZL-a(R550) continued to increase while higher reactivation temperature at 700 caused a significant drop in surface Pd content.

### 2.5. Dynamic Oxygen Storage/Release Capacity

The tolerability to air/fuel ratio fluctuation was considered one important aspect of TWC catalysts; therefore, the dynamic oxygen storage/release capacity (named DOSC) of the bimetallic catalysts was characterized by conducting CO-O<sub>2</sub> pulse tests at 200 °C/400 °C conditions. The obtained results are presented in Figure 6. Figure 6A exhibited two major peaks for CO<sub>2</sub> response curves. The first peak occurring within 0 to 10 s was designed as CO<sub>2</sub> (1) and the peak as CO<sub>2</sub> (2) was within 10–20 s. CO<sub>2</sub> (1) arose from the reaction between CO and active surface oxygen species upon CO injection. Compared to the fresh catalyst, the CO<sub>2</sub> response curves of 0.6Pt-0.4Pd/CZL-a sample descended quite clearly especially for the CO<sub>2</sub> (1) peak, suggestive of its deteriorated DOSC after thermal ageing. After reactivating at 550 °C, the CO<sub>2</sub> (1) peak of 0.6Pt-0.4Pd/CZL-a(R550) rose gently. While O<sub>2</sub> was injected, the observation of CO<sub>2</sub> (2) could be attributed to the decomposition of carbonates, which were formed due to the adsorption of CO on the Ce<sup>3+</sup> sites [26]. Thus, the CO<sub>2</sub> (2) peak of 0.6Pt-0.4Pd/CZL-a(R550) with higher Ce<sup>3+</sup> was largely recovered compared to that of 0.6Pt-0.4Pd/CZL-a and 0.6Pt-0.4Pd/CZL-a(R700) samples. When testing at 400 °C, the migration of lattice oxygen was accelerated and the adsorption of carbonate species became weaker; therefore, CO<sub>2</sub> (1) and CO<sub>2</sub> (2) basically merged into a single peak. The overall DOSC tested at 400 °C followed a similar order as that

tested at 200 °C: 0.6Pt-0.4Pd/CZL > 0.6Pt-0.4Pd/CZL-a(R550) > 0.6Pt-0.4Pd/CZL-a > 0.6Pt-0.4Pd/CZL-a(R700). These results demonstrated that the DOSC of aged catalyst reactivated at 550 °C can be effectively recovered due to the formation of more oxygen vacancies as well as restoration of PM–support interactions; whereas, reactivating at 700 °C caused decreasing surface PM content, thus leading to inferior DOSC.

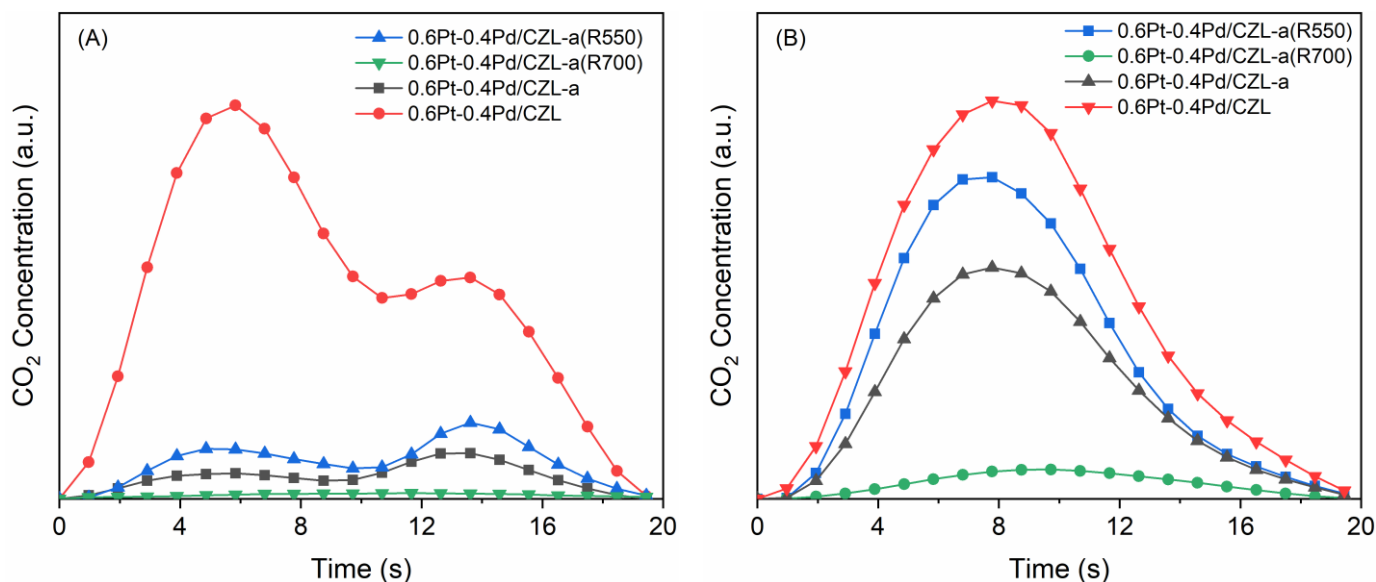


**Figure 6.** CO<sub>2</sub> response curves of 0.6Pt-0.4Pd/CZL, 0.6Pt-0.4Pd/CZL-a, 0.6Pt-0.4Pd/CZL-a(R550), and 0.6Pt-0.4Pd/CZL-a(R700) catalysts tested at (A) 200 °C and (B) 400 °C.

### 2.6. Redox Properties by H<sub>2</sub>-TPR

The redox properties of the fresh, aged, and reactivated catalysts were characterized through the H<sub>2</sub>-TPR tests, as Figure 7 depicted. The fresh 0.6Pt-0.4Pd/CZL showed two major reduction peaks named peak  $\alpha$  and peak  $\beta$ . Peak  $\alpha$  is attributed to the H<sub>2</sub> consumption by the PdO<sub>x</sub> species with the strong CZL support interaction, while peak  $\beta$  was ascribed to the reduction in PtO<sub>x</sub> species strongly interacted with CZL support [27]. Due to the existing hydrogen spillover effect [28], the hydrogen consumption of both peak  $\alpha$  and peak  $\beta$  over all the samples exceeded the theoretical value. For peak  $\alpha$ , the hydrogen consumption follows the order as 0.6Pt-0.4Pd/CZL(288.5  $\mu\text{mol/g-cat}$ ) > 0.6Pt-0.4Pd/CZL-a(R700)(257.6  $\mu\text{mol/g-cat}$ ) > 0.6Pt-0.4Pd/CZL-a(R550)(196.0  $\mu\text{mol/g-cat}$ ) > 0.6Pt-0.4Pd/CZL-a(191.6  $\mu\text{mol/g-cat}$ ); while that of peak  $\beta$  followed the order as 0.6Pt-0.4Pd/CZL-a(R550)(374.3  $\mu\text{mol/g-cat}$ ) > 0.6Pt-0.4Pd/CZL(372.4  $\mu\text{mol/g-cat}$ ) > 0.6Pt-0.4Pd/CZL-a(R700)(219.42  $\mu\text{mol/g-cat}$ ) > 0.6Pt-0.4Pd/CZL-a(37.0  $\mu\text{mol/g-cat}$ ). After thermal aging, the hydrogen consumption of peak  $\alpha$  decreased significantly, while the hydrogen consumption of peak  $\beta$  dropped to about 1/10 compared to the fresh sample. Moreover, a new reduction peak ( $\alpha'$ ) around 0 °C appeared on 0.6Pt-0.4Pd/CZL-a, which was assigned to the reduction in surface dispersed PMO<sub>x</sub> particles. These phenomena indicated that the PM–support interactions (especially the Pt-Ce interactions) were clearly weakened after thermal aging, which therefore led to a hindered hydrogen spillover effect. After reactivating at 550 °C, the hindered Pt-CZL interaction was significantly restored and enhanced according to the hydrogen consumption value of peak  $\beta$  but a similar improving effect regarding Pd-CZL interaction was hardly observed. For catalyst reactivated at 700 °C, the interaction between Pd and CZL support could be generally enhanced to a certain extent based on the hydrogen consumption value of peak  $\alpha$ . Whereas, a large proportion of metallic Pt<sup>0</sup> appeared rather than forming stable Pt-O-Ce species since PtO<sub>x</sub> would already start to decompose at such high temperatures.

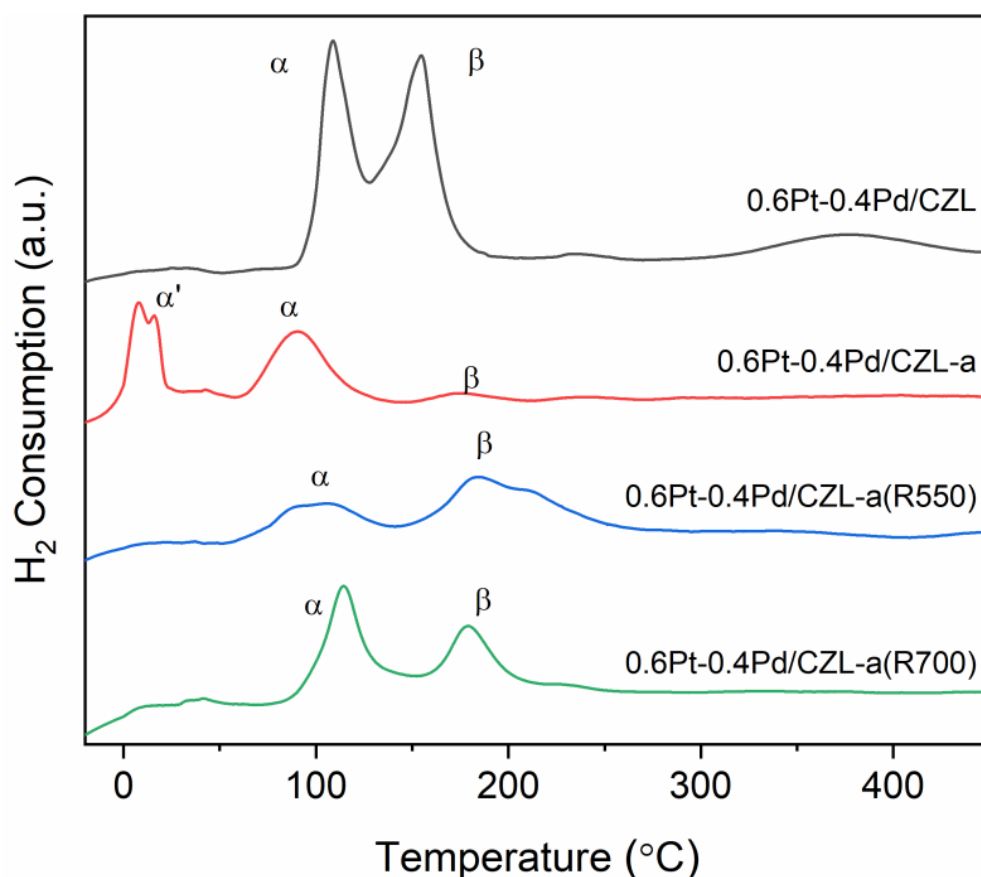


**Figure 7.** H<sub>2</sub>-TPR profiles of 0.6Pt-0.4Pd/CZL, 0.6Pt-0.4Pd/CZL-a, 0.6Pt-0.4Pd/CZL-a(R550), and 0.6Pt-0.4Pd/CZL-a(R700) catalysts.

### 2.7. Stability of Surface PMO<sub>x</sub> Species by O<sub>2</sub>-TPSR

To acquire more insights into the correlations between reactivation temperature and thermal stability of surface PMO<sub>x</sub> species, O<sub>2</sub>-TPSR experiments were conducted and the obtained profiles are shown in Figure 8. Three major peaks could be observed as peak  $\alpha$  around 500 °C, peak  $\beta$  around 1070 °C, and peak  $\gamma$  around 700 °C during the cooling process. By comparing the O<sub>2</sub>-TPSR profile of reference sample Pt/CZL and Pd/CZL, peak  $\alpha$  could be attributed to the oxygen-releasing peak due to the decomposition of PtO<sub>x</sub> species and peak  $\beta$  was ascribed to the oxygen-releasing peak due to the decomposition of PdO<sub>x</sub> species, whereas, peak  $\gamma$  was assigned to the oxygen consumption peak due to oxidation of metallic Pd during the cooling process [29,30]. It was quite clear that the PtO<sub>x</sub> species were relatively less stable and decomposed at relatively low temperatures, which explained why the metallic Pt<sup>0</sup> content on the catalyst surface increased after reactivating at 700 °C. For the bimetallic 0.6Pt-0.4Pd/CZL catalyst, both peak  $\alpha$  and peak  $\beta$  slightly shifted to a higher temperature, indicating that the stability of both PtO<sub>x</sub> and PdO<sub>x</sub> were enhanced. After thermal aging, the oxygen-releasing peak of PMO<sub>x</sub> decomposition became quite small and the decomposition temperatures were also significantly lower. These phenomena suggest that surface Pt and Pd species were severely sintered during thermal aging along with strongly hindered PM–support interactions. For 0.6Pt-0.4Pd/CZL-a(R550), the decomposition temperature of PtO<sub>x</sub> was increased, which once again proves that the interaction between Pt and CZL support was restored by reactivating at 550 °C.

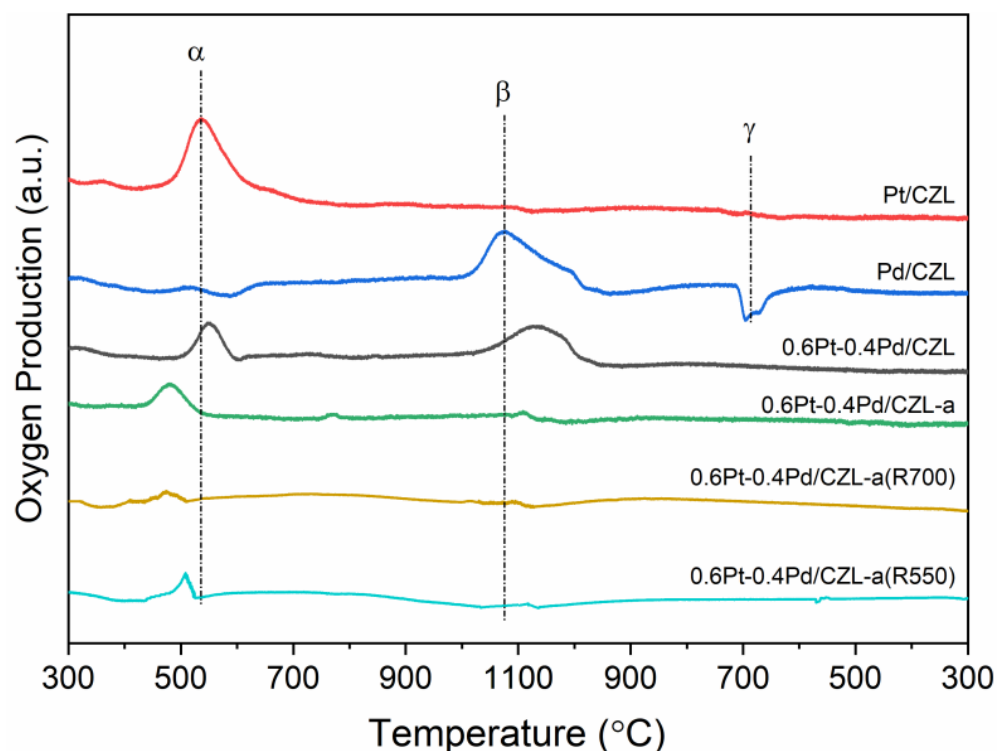


**Figure 8.** O<sub>2</sub>-TPSR profiles of Pt/CZL, Pd/CZL, 0.6Pt-0.4Pd/CZL, 0.6Pt-0.4Pd/CZL-a, 0.6Pt-0.4Pd/CZL-a(R550), and 0.6Pt-0.4Pd/CZL-a(R700) catalysts.

### 3. Experimental

#### 3.1. Catalyst Preparation

Bimetallic Pt-Pd catalysts were supported by the mixed oxides of CeO<sub>2</sub>-ZrO<sub>2</sub>-La<sub>2</sub>O<sub>3</sub> (including 40.3% CeO<sub>2</sub>, 49.5% ZrO<sub>2</sub>, and 5.1% La<sub>2</sub>O<sub>3</sub>), which are also denoted as CZL, using the conventional impregnation method for preparation (synthesis schematic shown in Figure S1). First, a quantitative amount of Pt(NO<sub>3</sub>)<sub>2</sub> and Pd(NO<sub>3</sub>)<sub>2</sub> solution (Analytical Reagent, Sinopharm Chemical Reagent Co., Ltd., Beijing, China) was added into CZL powders (Analytical Reagent, Solvay Rare Earth New Materials Co., Ltd., Liyang, China) combined with 20 mL distilled water and stirred for 3 h at 300 r/min speed. Following this, the resulting suspension was subjected to a 2 h period of drying at 100 °C, mortar-grounded, and then calcined at 500 °C under an air atmosphere for an additional 2 h. The total PM loading was 0.5 wt% and the obtained Pt-Pd bimetallic catalysts are denoted as 0.6Pt-0.4Pd/CZL, the optimized Pt/Pd ratio was namely selected as 4:1 based on our previous study regarding Pt-Pd/CZL bimetallic catalysts with various Pt/Pd ratios [12].

The fresh 0.6Pt-0.4Pd/CZL catalyst was then heated up to 1000 °C in air and kept for 2 h to obtain the thermal-aged sample (denoted as 0.6Pt-0.4Pd/CZL-a).

The aged 0.6Pt-0.4Pd/CZL-a sample was eventually subjected to the reactivating procedure as follows: 1 g of 0.6Pt-0.4Pd/CZL-a sample was loaded into a quartz tube and treated at a certain reactivation temperature for 2 h under a gas mixture of “16% O<sub>2</sub> + 10% H<sub>2</sub>O + 10% CO<sub>2</sub>” with N<sub>2</sub> as balancing gas. The reactivation temperatures ranged from 500 °C to 700 °C with 50 °C as an interval. Hence, the reactivated catalysts were labeled as 0.6Pt-0.4Pd/CZL-a (R500), 0.6Pt-0.4Pd/CZL-a (R550), 0.6Pt-0.4Pd/CZL-a (R600), 0.6Pt-0.4Pd/CZL-a (R650), and 0.6Pt-0.4Pd/CZL-a (R700).

#### 3.2. Three-Way Catalytic Performance Evaluations

The effectiveness of the three-way catalytic converter was evaluated using a custom-made micro-reactor with a temperature programming tool equipped. The synthetic gas was introduced at the point of stoichiometry, which consisted of C<sub>3</sub>H<sub>6</sub> with an 1100 ppm

value, C<sub>3</sub>H<sub>8</sub> with a 400 ppm precision, CO with a 15,000 ppm value, O<sub>2</sub> as 12,450 ppm precision, NO with a 1600 ppm precision, and NO<sub>2</sub> as 1200 ppm precision, with a balancing gas as Ar. This simulated gas was introduced under 0.2 mL of catalysts loaded into a quartz tube at a 38,700 h<sup>-1</sup> GHSV rate. The reactor temperature was ramped at a heating rate of 10 °C/min until the target point and 30 min stabilized. Subsequently, the outlet gas was analyzed by the application of a Nicolet IS50 FTIR instrument (manufactured by Thermo Fisher Scientific, Waltham, MA, USA.), including a multiple reflection gas cell and a ZnSe window.

The dynamic operation window was also determined under different air-to-fuel ratios at 400 °C. The air/fuel ratio  $\lambda$  was defined as  $(2[\text{O}_2] + 2[\text{NO}_2] + [\text{NO}]) / (10[\text{C}_3\text{H}_8] + 9[\text{C}_3\text{H}_6] + [\text{CO}])$  and it was adjusted from 0.90 to 1.15 by changing the oxygen concentration in the reaction gas mixture.

### 3.3. Catalyst Characterization

The images of catalysts observed via a high-resolution transmission electron microscope (HRTEM) were captured using a JEM 2100F instrument (manufactured by JEOL Ltd., Tokyo, Japan), incorporating EDS equipment. Before HRETM observation, the samples were dispersed into ethanol via supersonic treatment and then dripped onto a carbon film with the Cu grid supported.

X-ray photoelectron spectroscopy (XPS) analysis was performed on a Thermo ESCALAB 250 X-ray photoelectron spectrometer (Thermo Fisher Scientific, Waltham, MA, USA) equipped with monochromate Al K $\alpha$  radiation. The binding energies were calibrated using the C 1 s peak at 284.8 eV.

The dynamic oxygen storage/release capacity (DOSC) of the catalysts was determined using the CO-O<sub>2</sub> pulse method. The tests were conducted on an FD-2040 fixed-bed reactor (manufactured by Huasi Instrument Co., Ltd., Changsha, China). Initially, 50 mg of catalysts was pre-purged by Ar (with 97.5 mL/min flow rate) at 200 °C and pre-oxidized by O<sub>2</sub> (with 1.95 mL/min flow rate) for 15 min at the same temperature. Subsequently, pulses (at a 0.05 Hz frequency) of 13% CO/Ar and 6.5% O<sub>2</sub>/Ar were injected into the reactor alternately. A mass spectrometer HIDEN QIC-20 (manufactured by Hiden Analytical, Warrington, England, UK) was used to analyze the concentration of CO, O<sub>2</sub>, and CO<sub>2</sub> in the outlet gas.

H<sub>2</sub> temperature-programmed reduction (H<sub>2</sub>-TPR) tests were conducted in the Chem-BET PULSAR chemisorption apparatus (manufactured by Quantachrome Instruments, Boynton Beach, FL, USA). A 50 mg sample was purged by N<sub>2</sub> flow at 200 °C for 30 min before tests and then cooled down to -20 °C using liquid nitrogen. Then, 5 vol.% H<sub>2</sub>/Ar flow (40 mL/min) was introduced into the reactor until the baseline was stable. The H<sub>2</sub>-TPR profiles were recorded by monitoring H<sub>2</sub> consumption using thermal conductivity detector (TCD) signals while simultaneously raising the reactor temperature to 600 °C (heating rate of 10 °C/min).

O<sub>2</sub> temperature-programmed surface reaction (O<sub>2</sub>-TPSR) was conducted on a GC-1690 gas chromatograph employed with a TCD detector (manufactured by KeXiao Instrument Co., Ltd., Hangzhou, China). In total, a 100 mg catalyst was pretreated in N<sub>2</sub> flow (40 mL/min) at 500 °C for 30 min and then cooled to room temperature. The reaction flow was then switched to 2% O<sub>2</sub>/He (40 mL/min) and a stable baseline was waited for. The O<sub>2</sub>-TPSR profiles were obtained by monitoring the TCD signal while heating the sample to 1100 °C with a heating rate of 20 °C/min followed by cooling down to 300 °C with the same rate.

## 4. Conclusions

In this study, Pt-Pd bimetallic catalysts (0.6Pt-0.4Pd/CZL) were synthesized, thermally aged, and finally reactivated at different temperatures. The TWC catalytic activity and dynamic operation windows of the obtained catalysts were evaluated. Detailed characterizations including HRTEM, XPS, DOSC, H<sub>2</sub>-TPR, and O<sub>2</sub>-TPSR were conducted to study structural/chemical changes of the catalysts before and after reactivation treatment and to

explore possible reasons for activity recovery by reactivation treatment. Results show that reactivating at proper temperatures could effectively restore the TWC catalytic performance and widen the operation window width, as 0.6Pt-0.4Pd/CZL-a(R550) shows the best TWC activity recovery along with broadened operation temperature width. By reactivating at the appropriate temperature, the surface PM content was increased and the PM-support interaction could be restored; therefore, the redox properties and DOCS could be improved. However, reactivating at higher temperatures (i.e., 700 °C) caused encapsulation of Pd by CZL support and had limited effect on improving the Pt-CZL interaction, thus leading to inferior DOCS and TWC activity after reactivation.

**Supplementary Materials:** The following supporting information can be downloaded at <https://www.mdpi.com/article/10.3390/catal14050299/s1>. Figure S1: Synthesis scheme of the Pt-Pd/CZL catalysts; Figure S2: XRD patterns of the 0.6Pt-0.4Pd/CZL, 0.6Pt-0.4Pd/CZL-a, and 0.6Pt-0.4Pd/CZL-a(R550) catalysts; Table S1: Comparison of the reactivation protocols and results in this work with other reports. References [31–34] are cited in the Supplementary Materials.

**Author Contributions:** Conceptualization, J.W., K.C. and R.Z.; methodology, K.C., Q.S. and X.W.; validation, K.C., J.W., Y.L. and R.Z.; investigation, K.C., J.Z., Y.Z. and X.W.; resources, J.D., G.W. and R.Z.; data curation, K.C., J.D. and Y.L.; writing—original draft preparation, J.W.; writing—review and editing, J.W., G.W., Y.Z. and R.Z.; visualization, Q.S., J.Z., J.D., Y.Z. and X.W.; supervision, R.Z.; project administration, R.Z.; funding acquisition, Q.S., Y.L., G.W. and R.Z. All authors have read and agreed to the published version of the manuscript.

**Funding:** This work was supported by the National Key Research and Development Program of China (2022YFB3504200), Jiangsu Province Science and Technology Plan Special Fund (BZ2022053), Key Research and Development Program of Anhui Province (202104g01020006), the Scientific Research Fund of Nanjing Institute of Technology (QKJ202304, YKJ202047, and YKJ202048), and the Provincial key project of Innovation and Entrepreneurship Training Program for College Students in Jiangsu Province (202311276007Z).

**Data Availability Statement:** Data will be available on request.

**Conflicts of Interest:** The authors declare no conflicts of interest.

## References

1. Joshi, A. Review of vehicle engine efficiency and emissions. *SAE Int. J. Adv. Curr. Prac. Mobil.* **2019**, *1*, 734–761. [[CrossRef](#)]
2. Dey, S.; Mehta, N.S. Automobile pollution control using catalysis. *Resour. Environ. Sustain.* **2020**, *2*, 100006. [[CrossRef](#)]
3. Zhao, J.; Sun, J.; Meng, X.; Li, Z. Recent advances in vehicle exhaust treatment with photocatalytic technology. *Catalysts* **2022**, *12*, 1051. [[CrossRef](#)]
4. Robles-Lorite, L.; Dorado-Vicente, R.; Torres-Jiménez, E.; Bombek, G.; Lešnik, L. Recent advances in the development of automotive catalytic converters: A systematic review. *Energies* **2023**, *16*, 6425. [[CrossRef](#)]
5. Gao, S.Y.; Yu, D.; Zhou, S.R.; Zhang, C.L.; Wang, L.Y.; Fan, X.Q.; Yu, X.H.; Zhao, Z. Construction of cerium-based oxide catalysts with abundant defects/vacancies and their application to catalytic elimination of air pollutants. *J. Mater. Chem.* **2023**, *11*, 19210–19243. [[CrossRef](#)]
6. Vlachou, M.C.; Marchbank, H.R.; Brooke, E.; Kolpin, A. Challenges and opportunities for platinum in the modern three-way catalyst: Flexibility and performance in gasoline emissions control. *Johns. Matthey Tech.* **2023**, *67*, 219–229. [[CrossRef](#)]
7. Wang, J.H.; Chen, H.; Hu, Z.C.; Yao, M.F.; Li, Y.D. A review on the Pd-based three-way catalyst. *Catal. Rev.* **2015**, *57*, 79–144. [[CrossRef](#)]
8. Singh, A.K.; Xu, Q. Synergistic catalysis over bimetallic alloy nanoparticles. *ChemCatChem* **2013**, *5*, 652–676. [[CrossRef](#)]
9. Vedyagin, A.A.; Stoyanovskii, V.O.; Kenzhin, R.M.; Slavinskaya, E.M.; Plyusnin, P.E.; Shubin, Y.V. Purification of gasoline exhaust gases using bimetallic Pd-Rh/ $\delta$ -Al<sub>2</sub>O<sub>3</sub> catalysts. *React. Kinet. Mech. Cat.* **2019**, *127*, 137–148. [[CrossRef](#)]
10. Lim, B.; Jiang, M.; Camargo, P.H.C.; Cho, E.C.; Tao, J.; Lu, X.M.; Zhu, Y.M.; Xia, Y.N. Pd-Pt bimetallic nanodendrites with high activity for oxygen reduction. *Science* **2009**, *324*, 1302–1305. [[CrossRef](#)]
11. Jin, X.; Zhao, M.; Vora, M.; Shen, J.; Zeng, C.; Yan, W.J.; Thapa, P.S.; Subramaniam, B.; Chaudhari, R.V. Synergistic effects of bimetallic PtPd/TiO<sub>2</sub> nanocatalysts in oxidation of glucose to glucaric acid: Structure dependent activity and selectivity. *Ind. Eng. Chem. Res.* **2016**, *55*, 2932–2945. [[CrossRef](#)]
12. Chen, K.; Wan, J.; Wang, T.; Sun, Q.; Zhou, R.X. Construction of bimetallic Pt-Pd/CeO<sub>2</sub>-ZrO<sub>2</sub>-La<sub>2</sub>O<sub>3</sub> catalysts with different Pt/Pd ratios and its structure-activity correlations for three-way catalytic performance. *J. Rare Earths.* **2023**, *41*, 896–904. [[CrossRef](#)]
13. Datye, A.K.; Votsmeier, M. Opportunities and challenges in the development of advanced materials for emission control catalysts. *Nat. Mater.* **2021**, *20*, 1049–1059. [[CrossRef](#)] [[PubMed](#)]

14. Chen, X.Y.; Cheng, Y.S.; Seo, C.Y.; Schwank, J.W.; McCabe, R.W. Ageing, re-dispersion, and catalytic oxidation characteristics of model Pd/Al<sub>2</sub>O<sub>3</sub> automotive three-way catalysts. *Appl. Catal. B Environ.* **2015**, *163*, 499–509. [[CrossRef](#)]
15. Zhou, J.B.; Zhao, J.P.; Zhang, J.L.; Zhang, T.; Ye, M.; Liu, Z.M. Regeneration of catalysts deactivated by coke deposition: A review. *Chin. J. Catal.* **2020**, *41*, 1048–1061. [[CrossRef](#)]
16. Hickey, N.; Fornasiero, P.; Monte, R.D.; Kašpar, J.; González-Velasco, J.R.; Gutiérrez-Ortiz, M.A.; González-Marcos, M.P.; Gatica, J.M.; Bernal, S. Reactivation of aged model Pd/Ce<sub>0.68</sub>Zr<sub>0.32</sub>O<sub>2</sub> three-way catalyst by high temperature oxidising treatment. *Chem. Commun.* **2004**, *2*, 196–197. [[CrossRef](#)] [[PubMed](#)]
17. Nagai, Y.; Dohmae, K.; Ikeda, Y.; Takagi, N.; Tanabe, T.; Hara, N.; Guilera, G.; Pascarelli, S.; Newton, M.A.; Kuno, O.; et al. In situ redispersion of platinum autoexhaust catalysts: An on-line approach to increasing catalyst lifetimes. *Angew. Chem. Int. Ed* **2008**, *47*, 9303–9306. [[CrossRef](#)] [[PubMed](#)]
18. Eichler, A. CO oxidation on transition metal surfaces: Reaction rates from first principles. *Surf. Sci.* **2002**, *498*, 314–320. [[CrossRef](#)]
19. Wan, I.; Lin, J.S.; Guo, X.L.; Wang, T.; Zhou, R.X. Morphology effect on the structure-activity relationship of Rh/CeO<sub>2</sub>-ZrO<sub>2</sub> catalysts. *Chem. Eng. J.* **2019**, *368*, 719–729. [[CrossRef](#)]
20. Wu, Y.N.; Liao, S.J.; Su, Y.L.; Zeng, J.H.; Dang, D. Enhancement of anodic oxidation of formic acid on palladium decorated Pt/C catalyst. *J. Power Sources* **2010**, *195*, 6459–6462. [[CrossRef](#)]
21. Chen, S.Y.; Li, S.D.; You, R.Y.; Guo, Z.Y.; Wang, F.; Li, G.X.; Yuan, W.T.; Zhu, B.E.; Gao, Y.; Zhang, Z.; et al. Elucidation of active sites for CH<sub>4</sub> catalytic oxidation over Pd/CeO<sub>2</sub> via tailoring metal-support interactions. *ACS Catal.* **2021**, *11*, 5666–5677. [[CrossRef](#)]
22. Luo, Y.J.; Lin, D.F.; Zheng, Y.B.; Feng, X.S.; Chen, Q.H.; Zhang, K.; Wang, X.Y.; Jiang, L.L. MnO<sub>2</sub> nanoparticles encapsuled in spheres of Ce-Mn solid solution: Efficient catalyst and good water tolerance for low-temperature toluene oxidation. *Appl. Surf. Sci.* **2020**, *504*, 144481. [[CrossRef](#)]
23. Bozo, C.; Guilhaume, N.; Herrmann, J.M. Role of the ceria-zirconia support in the reactivity of platinum and palladium catalysts for methane total oxidation under lean conditions. *J. Catal.* **2001**, *203*, 393–406. [[CrossRef](#)]
24. Cao, K.; Cai, J.M.; Liu, X.; Chen, R. Catalysts design and synthesis via selective atomic layer deposition. *J. Vac. Sci. Technol. A* **2018**, *36*, 010801. [[CrossRef](#)]
25. Wang, B.; Weng, D.; Wu, X.D.; Ran, R. Modification of Pd-CeO<sub>2</sub> catalyst by different treatments: Effect on the structure and CO oxidation activity. *Appl. Surf. Sci.* **2011**, *257*, 3878–3883. [[CrossRef](#)]
26. Zhao, M.W.; Shen, M.Q.; Wang, J.; Wang, W.L. Influence of Pd morphology and support surface area on redox ability of Pd/Ce<sub>0.67</sub>Zr<sub>0.33</sub>O<sub>2</sub> under CO-He pulse and transient CO-O<sub>2</sub> Measurements. *Ind. Eng. Chem. Res.* **2007**, *46*, 7883–7890. [[CrossRef](#)]
27. Hickey, N.; Fornasiero, P.; Kašpar, J.; Gatica, J.M.; Bernal, S. Effects of the nature of the reducing agent on the transient redox behavior of NM/Ce<sub>0.68</sub>Zr<sub>0.32</sub>O<sub>2</sub> (NM=Pt, Pd, and Rh). *J. Catal.* **2001**, *200*, 181–193. [[CrossRef](#)]
28. Bernal, S.; Calvino, J.J.; Cauqui, M.A.; Gatica, J.M.; Larese, C.; Pérez Omil, J.A.; Pintado, J.M. Some recent results on metal/support interaction effects in NM/CeO<sub>2</sub> (NM: Noble metal) catalysts. *Catal. Today* **1999**, *50*, 175–206. [[CrossRef](#)]
29. Sinels'nikov, V.V.; Tolkachev, N.N.; Goryashchenko, S.S.; Telegina, N.S.; Stakheev, Y.A. Propane oxidation with chemically bound oxygen on Pt/TiO<sub>2</sub>/Al<sub>2</sub>O<sub>3</sub> and Pt/CeO<sub>2</sub>/Al<sub>2</sub>O<sub>3</sub> catalysts. *Kinet. Catal.* **2006**, *47*, 98–105. [[CrossRef](#)]
30. Lin, S.Y.; Yang, L.Y.; Yang, X.; Zhou, R.X. Redox behavior of active PdO<sub>x</sub> species on (Ce,Zr)<sub>x</sub>O<sub>2</sub>-Al<sub>2</sub>O<sub>3</sub> mixed oxides and its influence on the three-way catalytic performance. *Chem. Eng. J.* **2014**, *247*, 42–49. [[CrossRef](#)]
31. Anderson, J.A.; Daley, R.A.; Christou, S.Y.; Efstathiou, A.M. Regeneration of thermally aged Pt-Rh/Ce<sub>x</sub>Zr<sub>1-x</sub>O<sub>2</sub>-Al<sub>2</sub>O<sub>3</sub> model three-way catalysts by oxychlorination treatments. *Appl. Catal. B Environ.* **2006**, *64*, 189–200. [[CrossRef](#)]
32. Lambrou, P.S.; Polychronopoulou, K.; Petallidou, K.C.; Efstathiou, A.M. Oxy-chlorination as an effective treatment of aged Pd/CeO<sub>2</sub>-Al<sub>2</sub>O<sub>3</sub> catalysts for Pd redispersion. *Appl. Catal. B Environ.* **2012**, *111*, 349–359. [[CrossRef](#)]
33. Birgersson, H.; Eriksson, L.; Boutonnet, M.; Järås, S.G. Thermal gas treatment to regenerate spent automotive three-way exhaust gas catalysts (TWC). *Appl. Catal. B Environ.* **2004**, *54*, 193–200. [[CrossRef](#)]
34. Hatanaka, M.; Takahashi, N.; Tanabe, T.; Nagai, Y.; Dohmae, K.; Aoki, Y.; Yoshida, T.; Shinjoh, H. Ideal Pt loading for a Pt/CeO<sub>2</sub>-based catalyst stabilized by a Pt-O-Ce bond. *Appl. Catal. B Environ.* **2010**, *99*, 336–342. [[CrossRef](#)]

**Disclaimer/Publisher's Note:** The statements, opinions and data contained in all publications are solely those of the individual author(s) and contributor(s) and not of MDPI and/or the editor(s). MDPI and/or the editor(s) disclaim responsibility for any injury to people or property resulting from any ideas, methods, instructions or products referred to in the content.